Veröffentlichung

Autoren

Rossian, Lennart;Ewert, Roland;Delfs, Jan

Titel

Evaluation of Acoustic Jump Conditions at Discontinuous Porous Interfaces

Publisher o. Konferenz

AIAA AVIATION 2017, Denver, Paper 2017-3505

Jahr

2017

Internet-Link (Doi-Nr.)

https://arc.aiaa.org/doi/pdf/10.2514/6.2017-3505

Evaluation of Acoustic Jump Conditions at Discontinuous Porous Interfaces

L. Rossian* , R. Ewert† and J. W. Delfs‡

German Aerospace Center (DLR), D-38108 Braunschweig, Germany

Over the past years, the reduction of airfoil trailing edge noise has been addressed amongst others by the application of porous, permeable materials directly at the geometric edges, as these present a prominent noise source location. In experimental investigations, the beneficial influence of porous materials was found to be approximately 6 dB with a broadband nature. On the numerical side, with the approach of volume averaging a promising means to model complex porous materials has been found. Therewith, successful simulations have been run, that relate to experimental findings. In the following, an explicit modeling of the discontinuous interface between the porous material and the surrounding free flow by specific interface conditions was formulated. In the present paper an approach to evaluate different formulations of said interface conditions is presented and applied. The results are discussed concerning their physical background. Last, application simulations of a NACA0012 airfoil with solid and porous trailing edge are shown and compared to experimental data.

I. Introduction

Air traffic has continuously increased over the last decades and therefore aircraft noise has become a prominent topic in research and politics. With advances concerning engine related noise, airframe noise is no longer negligible when considering the overall aircraft noise. Thereby, one major contribution is the broadband turbulent boundary layer trailing edge noise (TBL-TEN). It is generated by interaction of turbulent eddies in the boundary layer of an airfoil with geometric discontinuities, for instance a pointed trailing edge. One promising and widely studied countermeasure is the application of trailing edge shape modifications similar to serrations. Moreover, Hayden and Chanaud[1] demonstrated that the application of porous material is reducing trailing edge noise. As a representation of such material, lengthwise slits applied to the trailing edge were analyzed in Ref. 2. The attained noise reduction is about 6 dB compared to the solid reference. Subsequently, the acoustic benefit of rigid, porous permeable materials, e.g. sintered metal fiber felts or metal foams was experimentally addressed. Therefore different materials were applied to the trailing edge of a high lift airfoil and aeroacoustically tested by Herr et al.[3] With this, a maximum sound reduction of about 6 dB to 8 dB has been reported.

The combination of Computational Aeroacoustics (CAA) and Computational Fluid Dynamics (CFD) is a proper approach to investigate the beneficial effects of porous structural elements on the acoustic near field of the object of interest in detail and therefore to develop a physical understanding. Over the last years, Faßmann et al.[4] and Rossian et al.[5] have shown that the beneficial influence of porous materials on trailing-edge noise can be numerically addressed. In a hybrid CFD/CAA procedure a stochastic source model to generate the broadband TBL-TEN was used. With this approach, the predicted overall noise reduction was found in accordance with the measurement. To enhance the simulation results and to address complex, meaning anisotropic and non-uniform materials, an advanced description of the interface between a porous material and the surrounding free flow has been formulated.[5]

In the present paper, an approach to evaluate different formulations of the interface conditions at porous edges is presented. Therefore, numerical test cases consisting of domains that are linked by different sets of

*PhD Student, Technical University Braunschweig, corresponding author lennart.rossian@dlr.de

†Senior Scientist, Senior AIAA Member

‡Head of Technical Acoustics Department, DLR Institute of Aerodynamics and Flow Technology, Professor for Technical Acoustics at TU Braunschweig Senior AIAA Member

equations are studied. With a plane wave and a monopole-like pressure source easy to analyze setups are provided that can be run at small computational costs. From the obtained results a suitable set of equations is chosen to be applied to actual trailing edge noise simulations with solid and porous materials.

II. Numerical Methods

In the following paragraphs the numerical methods used to model porous materials and their discontinuous interface with a surrounding free flow are briefly presented. In detail, a slightly modified formulation of the governing equations with respect to prior derivations[5] is introduced. Furthermore, an adjustment of the numerical implementation of the compact boundary scheme introduced in Ref. 5 is presented.

II.A. Volume averaged perturbation equations

To approach acoustic simulations of porous materials, two different paths can be pursued. The first possibility is to resolve the fine structure of such material and compute the acoustic variables inside the fluid regions.[6] Due to the small extension of the pores this leads to very fine computational meshes and therefore to computationally expensive simulations. The second possibility is to model the porous material by specific parameters and come up with a volume averaged formulation, as derived by Faßmann et al.[4] Investigating the effect of permeable materials on the noise generation, the detailed processes inside the material are of less interest than the overall interaction with the surrounding flow. Therefore, a representative description of the pores is suitable to vastly reduce the computational effort and thus provide the possibility to conduct design studies with different materials. One crucial aspect in this volume averaged description is the discontinuous edge of a porous regime. In the formula derived by Faßmann et al., a supposedly steady velocity has been introduced to deal with these discontinuities. Based on the Favre-averaged velocity $[v_i]$, the new variable $\hat{v}_i = \phi[v_i]$ was derived, with ϕ being the porosity, representing the volume ratio of fluid to total volume of the material. In the following it was revealed, that the edges of the porous regimes are to be addressed by specific jump conditions that allow the primitive variables to change discontinuously. Therefore, the continuous velocity is no longer needed. Next, the volume averaged Linearized Euler Equations are presented, which are obtained by volume averaging and subsequent Favre averaging of the velocities.

II.A.1. Volume averaged Linearized Euler Equations

The application of the above mentioned approach to a modified set of volume averaged variables without the artificial continuous velocity leads to the volume averaged Linearized Euler Equations (LEE). They read

continuity:
$$\begin{aligned}&\frac{\partial \rho'}{\partial t}+[v_i^0]\frac{\partial \rho'}{\partial x_i}+[v_i']\frac{\partial \rho^0}{\partial x_i}+\rho^0\frac{\partial [v_i']}{\partial x_i}+\rho'\frac{\partial [v_i^0]}{\partial x_i}-\dots\\ &\quad\underbrace{-\phi\left(\rho^0[v_i']+\rho'[v_i^0]\right)\frac{\partial}{\partial x_i}\frac{1}{\phi}}_{\text{gradient model term}}=S_\rho\end{aligned}\tag{1}$$

momentum:
$$\begin{aligned}&\frac{\partial [v_i']}{\partial t}+[v_j^0]\frac{\partial [v_i']}{\partial x_j}+[v_j']\frac{\partial [v_i^0]}{\partial x_j}+\frac{1}{\rho^0}\frac{\partial p'}{\partial x_i}-\frac{p'}{\rho^0\rho^0}\frac{\partial p^0}{\partial x_i}+\dots\\ &\quad+\underbrace{\phi\frac{\nu}{\kappa}\delta_{ij}[v_j']}_{\text{Darcy term}}+\underbrace{\phi^2\frac{c_\mathrm{F}}{\sqrt{\kappa}}\sqrt{[v_k^0][v_k^0]}\left[e_i^0e_j^0+\delta_{ij}\right][v_j']}_{\text{Forchheimer term}}-\dots\\ &\quad\underbrace{-\phi\frac{p'}{\rho^0}\frac{\gamma-1}{\gamma}\frac{\partial}{\partial x_i}\frac{1}{\phi}}_{\text{gradient model term}}=S_{v,i}\end{aligned}\tag{2}$$

energy:
$$\begin{aligned}&\frac{\partial p'}{\partial t}+[v_i^0]\frac{\partial p'}{\partial x_i}+[v_i']\frac{\partial p^0}{\partial x_i}+\gamma\left(p^0\frac{\partial [v_i']}{\partial x_i}+p'\frac{\partial [v_i^0]}{\partial x_i}\right)-\dots\\ &\quad\underbrace{-\phi p'\frac{\partial}{\partial x_i}\frac{1}{\phi}}_{\text{gradient model term}}=S_p\quad.\end{aligned}\tag{3}$$

Here, the variables ρ', v_i' and p' denote the acoustic fluctuating quantities, while ρ^0, v_i^0 and p^0 represent the underlying mean flow. Furthermore, κ is the isentropic exponent and the variables ϕ, κ and c_F describing the porous material are the porosity, permeability and the Forchheimer coefficient. The acoustic sources are provided for each equation by $S_{\rho;v,i;p}$. Note, that Eqs. (1) to (3) formulated with Favre averaged velocities take the exact form of the classic LEE with distinct additional terms for the treatment of the porous parameters. Furthermore, it can be easily seen, that if the porosity is chosen to $\phi = 1$ and the permeability tends to $\kappa \to \infty$ these terms vanish. Therefore, it can be stated that the reformulated form of the LEE provides a better legibility. As shown in Ref. 7, the description of the parameters κ and c_F as 3×3-tensors enables the modeling of anisotropic materials.

II.A.2. Volume averaged Acoustic Perturbation Equations

Besides the Linearized Euler Equations, the Acoustic Perturbation Equations (APE) are implemented in PIANO.[8] Here, a deviant momentum equation is realized to enable only the acoustic degrees of freedom to develop. The volume averaging and the additional porous terms are formulated analogously to the LEE. Hence, the new momentum equation reads:

$$\begin{aligned}
&\frac{\partial[v_i']}{\partial t} + \frac{\partial[v_k^0][v_k']}{\partial x_j} + \frac{1}{\rho^0}\frac{\partial p'}{\partial x_i} - \frac{p'}{\rho^0\rho^0}\frac{\partial p^0}{\partial x_i} + \dots \\
&\quad + \underbrace{\phi\frac{\nu}{\kappa}\delta_{ij}[v_j']}_{\text{Darcy term}} + \underbrace{\phi^2\frac{c_\mathrm{F}}{\sqrt{\kappa}}\sqrt{[v_k^0][v_k^0]}\left[e_i^0 e_j^0 + \delta_{ij}\right][v_j']}_{\text{Forchheimer term}} - \underbrace{\phi\frac{p'}{\rho^0}\frac{\gamma-1}{\gamma}\frac{\partial}{\partial x_i}\frac{1}{\phi}}_{\text{gradient model term}} = \dots \\
&\quad = -[\boldsymbol{\omega}'] \times [\boldsymbol{v}^0] - [\boldsymbol{\omega}^0] \times [\boldsymbol{v}'] + S_{v,i}
\end{aligned} \tag{4}$$

with ω' representing the fluctuating respectively ω^0 the mean vorticity.

II.B. Jump conditions at interfaces

When dealing with porous media in Computational Fluid Dynamics (CFD) simulations, the interface between regions of porous and free medium is modeled by specific jump conditions. This approach is based on the idea of invariant flow quantities not changing across the interface. Mößner et al.[9] describe the boundary conditions in the following way:

- Convective fluxes of mean flow equations are conserved.
- Diffusive fluxes of the mean flow equations are conserved.
- The flow change of the averaged quantities is isentropic.

Transferring this approach to the field of Computational Aeroacoustic (CAA) simulations, Rossian et al.[5] came up with a set of acoustic jump conditions, that play on the conservation of the

- mass flow
- energy
- entropy
- normal derivative of the energy
- normal derivative of the entropy

across the interface between the porous and the free flow. Furthermore, the normal derivatives of the velocities at the interface are allowed to jump according to a fixed relation. This can be physically related to surface stresses on the edge of the porous material. Like that, jump conditions are formulated, that provide a C^1 continuity of the chosen jump variables across the interface.

The derivation of interface conditions is performed similar to that of the LEE by the volume averaging approach, decomposition in steady and fluctuating variables and finally linearization. As before, the formulation with respect to that found by Rossian et al.[5] is modified due to the shift away from the quasi-continuous

velocities $\hat{v}_i$ to the Favre averaged variables $[v_i]$. For the link of the 5 acoustic variables ρ', v_i' and p' and their normal derivatives $\frac{\partial \rho'}{\partial n}$, $\frac{\partial v_i'}{\partial n}$ and $\frac{\partial p'}{\partial n}$ with respect to the interface, a set of 10 equations are required. So, the set of boundary conditions reads:

conservation of mass flow:
$$\rho' \phi[v_i^0] + \rho^0 \phi[v_i'] = \text{const.} \tag{5}$$

conservation of energy:
$$\frac{\gamma}{\gamma - 1}\left(\frac{p'}{\rho^0} - \frac{p^0 \rho'}{(\rho^0)^2}\right) + [v_i^0][v_i'] = \text{const.} \tag{6}$$

isentropy:
$$\frac{p'}{(\rho^0)^\gamma} - \gamma \frac{\rho' p^0}{(\rho^0)^{\gamma+1}} = \text{const.} \tag{7}$$

normal derivative of energy:
$$\begin{aligned} &\frac{\gamma}{\gamma - 1}\left(\frac{1}{\rho^0}\frac{\partial p'}{\partial n} - \frac{p'}{(\rho^0)^2}\frac{\partial \rho^0}{\partial n} - \frac{\rho'}{(\rho^0)^2}\frac{\partial p^0}{\partial n}\right) - \dots \\ &-\frac{\gamma}{\gamma - 1}\left(\frac{p^0}{(\rho^0)^2}\frac{\partial \rho'}{\partial n} - 2\frac{p^0 \rho'}{(\rho^0)^3}\frac{\partial \rho^0}{\partial n}\right) + \dots \\ &+[v_i']\frac{\partial [v_i^0]}{\partial n} + [v_i^0]\frac{\partial [v_i']}{\partial n} = \text{const.} \end{aligned} \tag{8}$$

jump of viscous stress:
$$\frac{\partial [v_i']}{\partial n} + (1 - \phi)\,\phi \frac{\beta}{\sqrt{\kappa}}[v_i'] = \text{const.} \tag{9}$$

normal derivative of isentropy:
$$\begin{aligned} &\frac{1}{(\rho^0)^\gamma}\frac{\partial p'}{\partial n} - \frac{\gamma \rho'}{(\rho^0)^{(\gamma+1)}}\frac{\partial p^0}{\partial n} - \frac{\gamma p'}{(\rho^0)^{(\gamma+1)}}\frac{\partial \rho^0}{\partial n} - \dots \\ &-\frac{\gamma p^0}{(\rho^0)^{(\gamma+1)}}\frac{\partial \rho'}{\partial n} + \frac{\gamma(\gamma+1)}{(\rho^0 \rho')^{(\gamma+2)}}\frac{\partial \rho^0}{\partial n} = \text{const.} \end{aligned} \tag{10}$$

Taking that Eq. (5) and Eq. (9) provide provide 3 components each, one comes up with the requested 10 equations. Eq. (9) provides a jump parameter β, that is undetermined a priori. Physically, this parameter models surface forces on the edge of the porous material, that yield a kink in the velocity profile at the interface.[9]

A modification of these jump equations for the primitive variables in the following analysis is to replace Eq. (9) by Eq. (11) below. By this, the equations for the normal derivatives of the primitive variables are based on the before considered continuous quantities (mass flow, energy and entropy). Furthermore, the use of the modeling parameter β and therefore the necessity to determine its value is avoided.

normal derivative of mass flow:
$$\begin{aligned} &\rho^0 [v_i']\frac{\partial \phi}{\partial n} + \rho' [v_i^0]\frac{\partial \phi}{\partial n} + \phi \rho^0 \frac{\partial [v_i']}{\partial n} + \phi [v_i']\frac{\partial \rho^0}{\partial n} + \dots \\ &+\phi \rho' \frac{\partial [v_i^0]}{\partial n} + \phi [v_i^0]\frac{\partial \rho'}{\partial n} = \text{const.} \end{aligned} \tag{11}$$

All the presented equations are shown in linearized form. This approach is usually valid, as the acoustic perturbation values are of significantly lower order than the mean flow quantities. To verify this assumption, the non-linear counterparts to the above listed jump conditions have been tested. To solve the non-linear set of equations, Newton's system has been implemented, that converges within 5 steps starting from equivalence of the primitive variables on both sides of the interface. Here, it was shown that the relative error of the linear equations lies in the order of magnitude of 10^{-5}. Resultant there is no need to solve the non-linear system in the typical regime of Mach-numbers considered in airframe noise problems.

II.C. Compact Boundary Scheme

On the numerical side, the interface is realized by a compact boundary scheme, as presented by Rossian et al.[5] This is feasible, as the porous regions are treated as individual blocks in the block structured formulation of PIANO. Figs. 1 and 2 illustrate the difference between the classic communication scheme via ghost points that enable to calculate the derivatives for the whole computational domain with a central 7-point DRP-stencil and the compact scheme.

For the compact formulation, the link between two different computational domains is changed to the direct communication of the function values and their a priori determined one sided stencil based normal

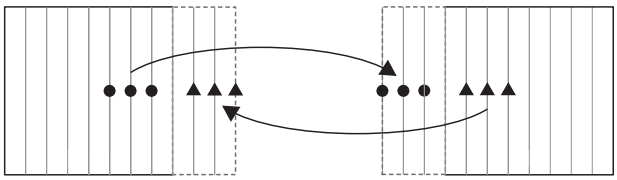

Figure 1. Schematic of the classic block to block communication scheme via ghost points.

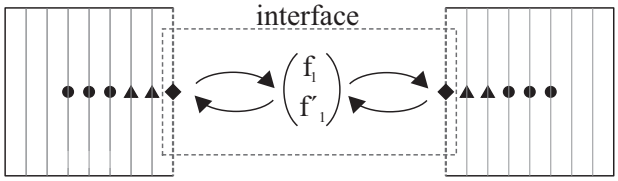

Figure 2. Schematic of the compact block to block communication scheme with the direct exchange of boundary value and derivative.

derivatives with respect to the interface. Then, the derivatives of the first two inner points of each block are calculated by Eq. (12) with the given derivative on the edge f'_1.

$$D\begin{pmatrix} f'_2 \\ f'_3 \\ f'_4 \end{pmatrix} = \frac{1}{\Delta}\begin{pmatrix} -\frac{a}{2} & 0 & \frac{a}{2} & 0 & 0 & 0 & 0 \\ 0 & -\frac{a}{2} & 0 & \frac{a}{2} & 0 & 0 & 0 \\ -a_3 & -a_2 & -a_1 & 0 & a_1 & a_2 & a_3 \end{pmatrix}\begin{pmatrix} f_1 \\ f_2 \\ f_3 \\ f_4 \\ f_5 \\ f_6 \\ f_7 \end{pmatrix} - \begin{pmatrix} \alpha \\ 0 \\ 0 \end{pmatrix} f'_1 \tag{12}$$

$$\text{with} \quad D = \begin{pmatrix} 1 & \alpha & 0 \\ \alpha & 1 & \alpha \\ 0 & 0 & 1 \end{pmatrix}, \quad \alpha = \frac{1}{4}, \quad a = \frac{3}{2}$$

Initially it was suggested, that the derivatives on the edge were to be calculated by a cut-in-half 7-point DRP-stencil, so that after averaging over both sides the original DRP-stencil is built. In the implementation process of the compact boundary scheme, it was revealed that the order of the single-sided differentiation stencil has to be reduced to preserve numerical stability. This is most relevant on curvilinear meshes. Therefore, a switch to a classical single-sided finite difference stencil of 2nd order on 3 points is made (cf. Eq. (13)). The effect of this local reduction in order will be studied in section IV.A.

$$f'_1 = \frac{1}{\Delta}(-1.5f_1 + 2f_{1+1} - 0.5f_{1+2}) \tag{13}$$

III. Basic Simulation Setup

To provide the ability to evaluate different jump conditions, several test cases are set up. These consist of a computational domain with a total extension of 201×101 grid points and a spacing of $\Delta x = \Delta y = 1$, being divided into two to three sub domains. The interfaces are realized by the particular jump conditions. As depicted in Fig. 3, the first test case consists of three blocks that are aligned successively. As an acoustic signal, a plane wave with a wavelength of 7 or 20 points traveling from left to right is passing through the domain. It is formulated by one wavelength of a sin-function according to Eq. (14).

$$\left.\begin{matrix} \rho'(x, t=0) \\ v'_i(x, t=0) \\ p'(x, t=0) \end{matrix}\right\} = \begin{cases} 2 \cdot 10^{-5} \sin\left(\frac{2\pi}{\lambda}(x-91)\right) & , x = [-91, (-91+\lambda)], \lambda = [7; 20] \\ 0 & , else \end{cases} \tag{14}$$

Along its way, it passes 2 block interfaces. Inside the computational domain, four microphones positioned on the centerline at $y = 51$ register the acoustic variables $\rho', u,' v'$ and p'. From the time signals and the resultant spectra the reflection and transmission properties of different interface formulations will be studied. Note, that all three blocks are given the same porosity parameters that relate to free flow (i.e. $\phi = 1$, $\kappa \to \infty$, $c_F = 0$).

From there on, in a second test series the differences between the interface formulations are to be evaluated. Fig. 4 sketches a test case consisting of two blocks with differing porosity parameters. As before, the acoustic test signal is a plane wave, now with a wavelength of 31 points, traveling from left to right through

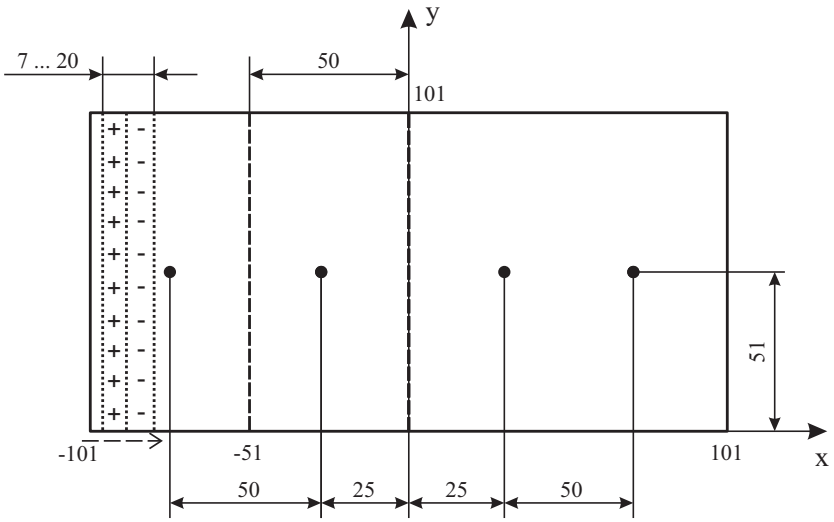

Figure 3. Schematic of the test case with three domains ($x \in [-101, -51], [-51, 0], [0, 101]$), plane wave passing two interfaces and four microphone positions along the center line of the computational domain.

the computational domain. For the analysis, the x-component of the acoustic intensity $\vec{I} = \overline{p'\vec{v'}}$ is calculated. With the plane wave, the intensity is directly proportional to the acoustic power, as the integration along the y-direction reduces to a simple scalar multiplication. Thus, the power conserving property of the chosen interface conditions can be evaluated directly. Hereby, it is important to consider the porosity ϕ of the right domain. As the acoustic variables are defined by a volume averaged presentation regarding the fluid part of the porous material, the integration has to be conducted over $\phi \cdot dy$. Consequently, in the following the intensity is always multiplied by ϕ.

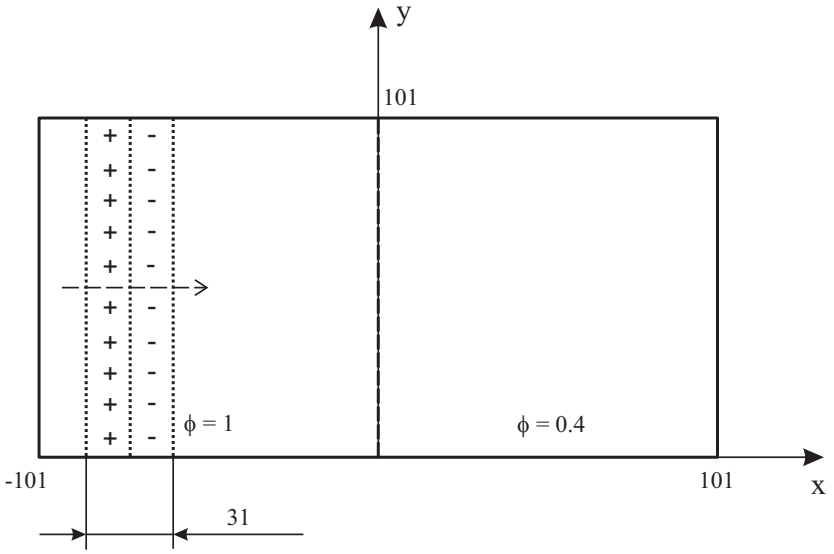

Figure 4. Schematic of the test case with two domains ($x \in [-101, 0], [0, 101]$) and plane wave traveling to the porous interface.

In the third setup (cf. Fig. 5), the acoustic source is changed to a Gaussian monopole pressure pulse, defined by Eq. (15). With analysis of both components of the acoustic intensity multiplied by the porosity, the reflection and transmission properties of the interface can be qualified concerning a non-orthogonal incoming wave. Note, that different from the case with the plane wave, here the calculated x-intensity does not account for the power transmitted over the whole domain, but only along the specific lines.

$$p'(x, t = 0) = 0.1 \exp\left[-\ln 2 \frac{(x_i - x_i^c)^2}{b^2}\right], x_x = -51, x_y = 51, b = 5 \tag{15}$$

To reduce the computational effort, no mean flow is considered in any of the test cases. Thereby one avoids

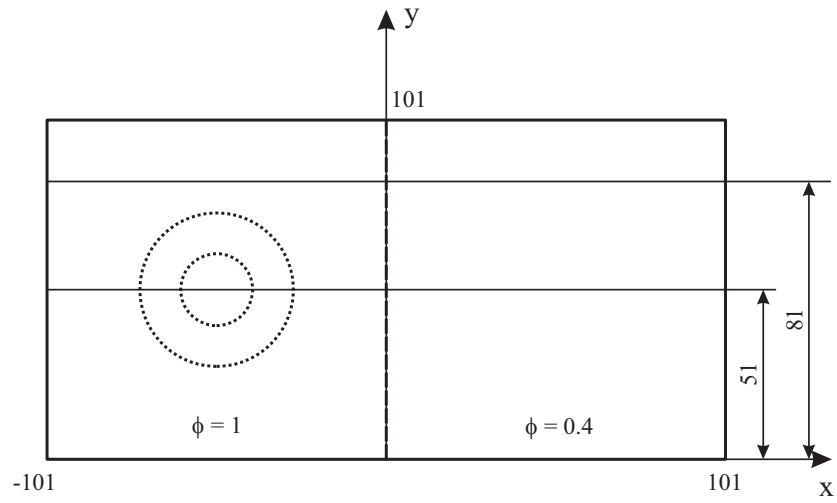

Figure 5. Schematic of the test case with two domains ($x \in [-101, 0], [0, 101]$), a monopole pressure pulse located in the domain of free flow and the two cuts to evaluate the acoustic field.

to first conduct CFD simulations and the effect of the different jump conditions on the acoustics is isolated. With this approach, the jump conditions presented in section II.B are reduced and when written in matrix formulation take the form of Eq. (16).

$$\mathbf{J} \cdot \begin{pmatrix} \rho' \\ [u'] \\ [v'] \\ [w'] \\ p' \\ \frac{\partial \rho'}{\partial n} \\ \frac{\partial [u']}{\partial n} \\ \frac{\partial [v']}{\partial n} \\ \frac{\partial [w']}{\partial n} \\ \frac{\partial p'}{\partial n} \end{pmatrix} = \text{const.} \tag{16}$$

$$\mathbf{J} = \begin{pmatrix} -\gamma \frac{p^0}{(\rho^0)^{(\gamma+1)}} & 0 & 0 & 0 & \frac{1}{(\rho^0)^\gamma} & 0 & 0 & 0 & 0 & 0 \\ 0 & \rho^0 & 0 & 0 & 0 & 0 & 0 & 0 & 0 & 0 \\ 0 & 0 & \rho^0 & 0 & 0 & 0 & 0 & 0 & 0 & 0 \\ 0 & 0 & 0 & \rho^0 & 0 & 0 & 0 & 0 & 0 & 0 \\ \frac{\gamma}{\gamma-1} \frac{p^0}{(\rho^0)^2} & 0 & 0 & 0 & 0 \frac{\gamma}{\gamma-1} \frac{1}{\rho^0} & 0 & 0 & 0 & 0 & 0 \\ 0 & 0 & 0 & 0 & 0 & -\frac{\gamma p^0}{(\rho^0)^{(\gamma+1)}} & 0 & 0 & 0 & 0 \frac{1}{(\rho^0)^\gamma} \\ 0 & (1-\phi)\phi \frac{\beta}{\sqrt{\kappa}} & 0 & 0 & 0 & 0 & 1 & 0 & 0 & 0 \\ 0 & 0 & (1-\phi)\phi \frac{\beta}{\sqrt{\kappa}} & 0 & 0 & 0 & 0 & 1 & 0 & 0 \\ 0 & 0 & 0 & (1-\phi)\phi \frac{\beta}{\sqrt{\kappa}} & 0 & 0 & 0 & 0 & 1 & 0 \\ 0 & 0 & 0 & 0 & 0 & -\frac{\gamma}{\gamma-1} \frac{p^0}{(\rho^0)^2} & 0 & 0 & 0 & \frac{\gamma}{\gamma-1} \frac{1}{\rho^0} \end{pmatrix}$$

IV. Basic Results

IV.A. Interface between identical domains

Before starting with the evaluation of the implemented jump conditions at the edge of a porosity, the influence of the reduced order of the single sided differentiation stencil is examined. The switch from a

4th order dispersion-relation-preserving scheme to a 2nd order standard finite difference scheme might have an effect on the propagation of the acoustic waves. Thus, in the following, the influence of the formulated compact boundary scheme is evaluated in comparison with the classic block-to-block communication via ghost points. The latter gives a solution that would be obtained if no interfaces are set at all and the wave was just traveling through the computational domain. Figs. 6 and 7 show the recorded narrow band spectra of the leftmost and rightmost of the four microphones positioned inside the three computational domains of the testcase shown in Fig. 3. The realized interface conditions were the classic exchange of the primitive variables with three ghost points on the one side and the presented jump conditions of section II.B with the compact boundary scheme on the other side. Hereby, a modification with respect to the formulation presented in II.B was tested by omitting the equations for the normal derivatives. Thus, just a C^0-continuous coupling of the domains is realized.

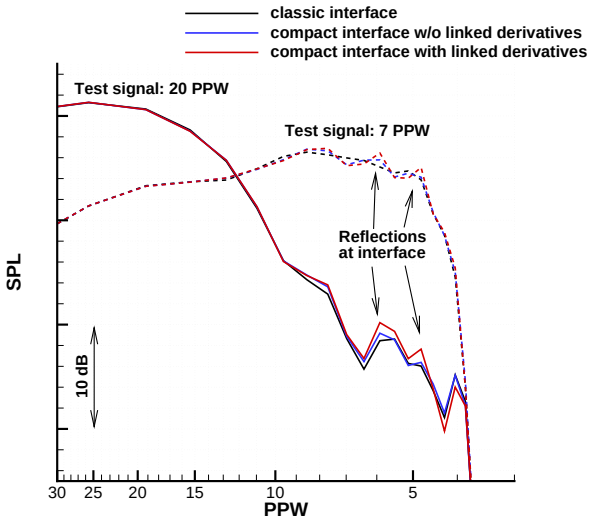

Figure 6. Narrow band spectra registered at leftmost microphone of the test case sketched in Fig. 3 for two different wavelengths and different formulation of the block interfaces.

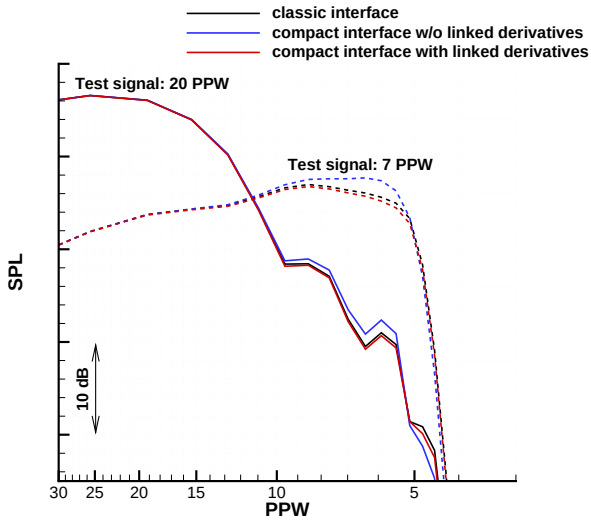

Figure 7. Narrow band spectra registered at rightmost microphone of the test case sketched in Fig. 3 for two different wavelengths and different formulation of the block interfaces

Fig. 6 shows the spectra of the registered signals at a position on the leftmost microphone at $x = -75$ for both test signals. Even at this point deviations of the new interface conditions with and without coupling of the derivatives from the classic formulation are already visible for both test signals. These are in the range of ± 1 dB and affect the high frequency range relating to resolutions of less than 10 points per wavelengths. A closer look into the simulation results animated over time reveals, that these deviations arise from spurious reflections at the first interface. It is interesting to notice, that the reflections are stronger with the coupling of the derivatives. It seems that by the use of the compact boundary scheme in combination with the reduced order scheme artificial forces are introduced. This is observed for the two test signals with different initial wavelengths. It is interesting to notice, that the effect of the artificial reflections appears in the same magnitude for both signals.

Furthermore, Fig. 7 shows the spectra of the test signals registered by the rightmost microphone at $x = 75$ for both test signals. Here, a more definite influence of the new interface conditions can be seen, which is still limited to high frequencies related to a resolution of less than 10 PPW. In contrast to the prior shown spectra, the deviation from the classic interface is higher when the derivatives are not considered. Here, the maximum error is an increase of the pressure level of about 2 dB at a resolution of 6 to 7 PPW. This seem appropriate, as with the given link of the derivatives the two separate stencils of each domain make up one stencil of greater extend. Therefore, the reduction of order might be decreased. As before, there is no basic difference in the effect of the interface the the two different test signals. Note, that for the test signal with 7 PPW, the increase of the sound pressure level in the regime of 5-8 PPW is stronger than for the test signal with 20 PPW. This is plausible, as for the longer wavelength less energy is contained in the high frequencies. Therefore, less energy is shifted to the lower frequencies.

From the shown spectra, one can derive that within specific limits the new interface formulations are well suited when it comes to domains with equal porosity parameters. If a link for the normal derivatives

of the considered variables is provided, the transmission across an interface is improved. However, in this case slightly more spurious reflections are generated. As all these drawbacks are strictly limited to a wave resolution of 10 points per wavelength and less in relation to the classic interface formulation with ghost points, it was shown that both new formulations remain valid candidates when dealing with an interface between domains of different porous parameters in the following.

IV.B. Interface between different porous domains

In what follows, different aspects concerning the formulation of the jump conditions in application to an interface between a porous material and a free flow are presented. First, the influence of the yet undetermined jump parameter β in Eq. (9) is discussed and then essentially different interface conditions are addressed.

IV.B.1. Influence of the jump parameter β

The first step in the evaluation of the acoustic jump conditions derived in II.B is to determine the influence of the jump parameter β. As β may take positive as well as negative values, both regimes were covered with exemplary simulations. Fig. 8 shows the acoustic intensity multiplied by ϕ in the vicinity of the porous interface for three exemplary values of β. It is shown that the choice of the jump parameter has notable effect on the characteristics of the interface conditions and therefore the whole acoustic field. It can be seen, that for $\beta = \pm 0.001$ significant perturbations of the acoustic intensity in the form of grid-to-grid oscillations appear. These occur whenever β is non-zero. During the tests, values down to $\beta = \pm 10^{-10}$ have been applied. For these, only deteriorations compared to the solution for $\beta = 0$ have been found. If furthermore the absolute value is of the order of 1 or greater, the simulation becomes unstable.

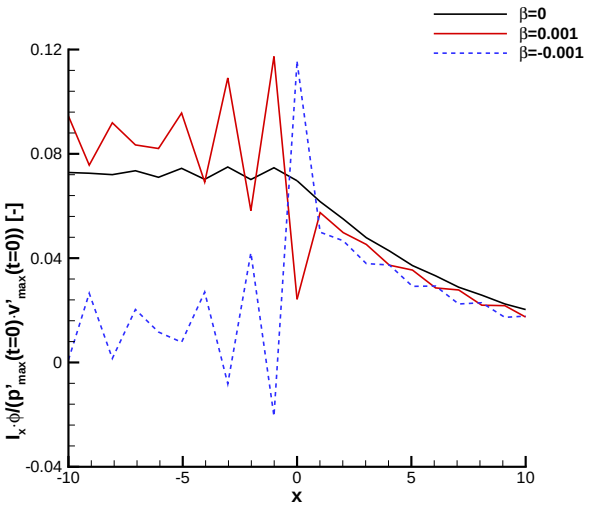

Figure 8. X-component of acoustic intensity across the domain interface for simulation with different jump parameters $\beta = 0$ and $\beta = \pm 0.001$

From this result, it can be derived that any further evaluation of fundamental changes in the formulation of the jump conditions are to be compared with the case of $\beta = 0$. Moreover, for later application simulations β would not need to be determined a priori. Thus, the jump conditions may be directly applied, while information about the topology of the interface, that is included in β, is indirectly taken into account by the underlying RANS mean flow field.

IV.B.2. Comparison between continuous and jump interface conditions

To evaluate the performance of different interface conditions, five different simulation setups are run. In the first one the primitive variables and their derivatives are considered as continuous variables across the interface. This is easily obtained by setting the jump matrix $\mathbf{J}$ from Eq. (16) equal to the unity matrix and therefore presents a simple approach to interface conditions. The successive simulations are conducted with the different jump equations from section II.B. Considering the preceding results, for the first set the

derivatives of the velocity are linked with the jump parameter $\beta = 0$. Then this equation is replaced by the conservation of the mass flow derivative. For the last step, no equation linking the derivatives of the two domains is considered.

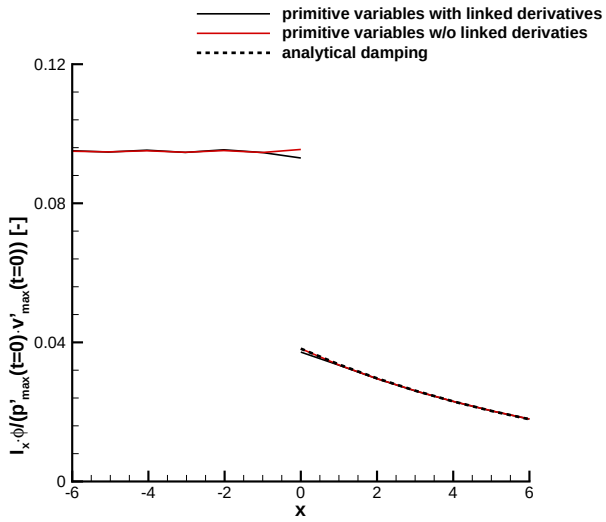

Figure 9. X**-component of acoustic intensity across the domain interface for simulation with conservation of primitive variables.**

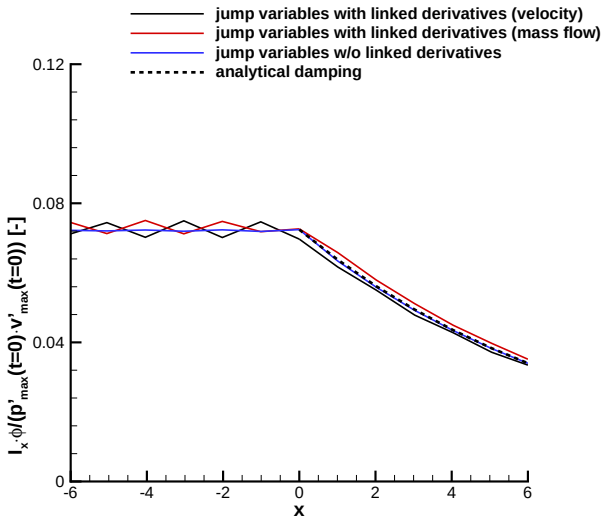

Figure 10. X**-component of acoustic intensity across the domain interface with different realizations of jump conditions.**

Fig. 9 shows the calculated acoustic intensity in the vicinity of the interface between the domain of free flow on the left and the porous domain on the right. It can be seen that across the interface a considerable intensity loss of 60% occurs. This relates directly to the chosen porosity of 0.4. As mentioned before, the acoustic variables in the volume averaged formulation are related to the fluid part of the porous material only. Therefore, the conservation of the primitive variables at the interface does not take into account the sudden effective reduction of the cross section due to the solid phase of the material. Hence, the acceleration of the fluid is not considered and this formulation is not suitable to describe the porous interface by its physical properties. Regardless this shortcut, it is interesting to have a look at the differences that are due to considering or omitting the link of the derivatives across the interface. It can be seen, that both solutions tend to small grid-to-grid oscillations inside the free flow domain with the same magnitude. The only difference here can be found on the exact point on the interface. The same holds for the porous domain, only that here no oscillations are visible. Furthermore, when comparing the damping inside the porous domain with the analytical damping compound from the damping of the pressure and velocity fluctuations (cf. Eq. (17)), the realization without link of the derivatives shows a better agreement. With the link for the derivatives, the calculated intensity declines less from the interface to the first inner point of the domain. This effect is limited to the very vicinity of the interface and therefore not relevant for the overall solution.

$$\left.\begin{matrix} \frac{\tilde{p}}{\tilde{p}_{max}}(x) \\ \frac{\tilde{v_i}}{\tilde{v_i}_{max}}(x) \end{matrix}\right\} = \exp(\lambda x) \tag{17}$$

$$x \in [0, 101]$$

$$\lambda = -\frac{\omega}{a_\infty}\sqrt{\frac{1}{2}\left(\sqrt{\frac{\phi\nu}{\kappa\omega^2}+1}-1\right)}$$

$$\tilde{p}_{max} = \tilde{p}(x=0)$$

$$\tilde{v_i}_{max} = \tilde{v_i}(x=0)$$

Alongside, Fig. 10 shows a different behavior for the jump conditions from section II.B. Here, all realizations show a continuous course of the acoustic intensity across the interface. This is the expected behavior, as in the calculation of the mass flow the blocking effect of the solid material phase is considered and furthermore, an explicit conservation of the energy is taken into account. In principle, these formulations therefore relate

to the physical understanding of such interface. Having a closer look on the formulation for treating the normal derivatives, considerable differences can be observed. As soon as a link for the derivatives is realized, prominent grid to grid oscillations appaer. Other than before, these are not limited to the very vicinity of the interface. For the case when the derivative of the velocity is linked directly, the oscillations are also visible inside the porous domain. For the case when the derivatives are independent on both sides of the interface, small oscillations are visible, too. However, these are significantly smaller than with the other realizations. Inside the porous domain, the damping again is in good agreement with the analytical solution. Altogether, the formulation of the interface conditions with the jump equations without coupling of the normal derivatives at the domain interface seems to be a meaningful choice for the case of acoustic waves with an incident angle of 90°.

To study the porous interface for non-orthogonal incidence, a Gaussian monopole pulse as show in Fig. 5 is simulated (cf. Eq. (15)). Figs. 11 and 12 show the x- and the y-component of the acoustic intensity multiplied by the porosity ϕ. Here, this is not representative for the acoustic power over the complete y-extend, but only for each cut with $y = \text{const.}$. Shown are two cuts, one at $y = 51$ in the middle of the domain and the other at $y = 81$ in the upper half of the domain. With the cut in the middle, where the incidence angle is 0 as before with the plane wave, a direct comparison with the preceding results is feasible. The second cut enables an analysis of the y-component of the acoustic intensity.

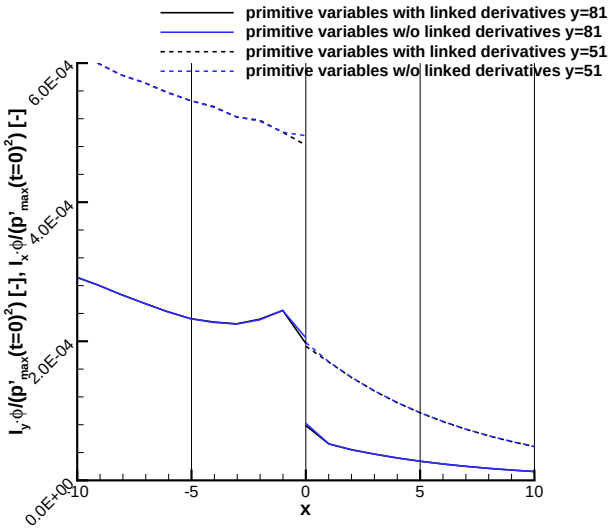

Figure 11. Acoustic intensity across the domain interface for simulation with conservation of primitive variables along two lines at $y = 51$ (dashed lines, x-component of intensity) and $y = 81$ (solid lines, y-component of intensity).

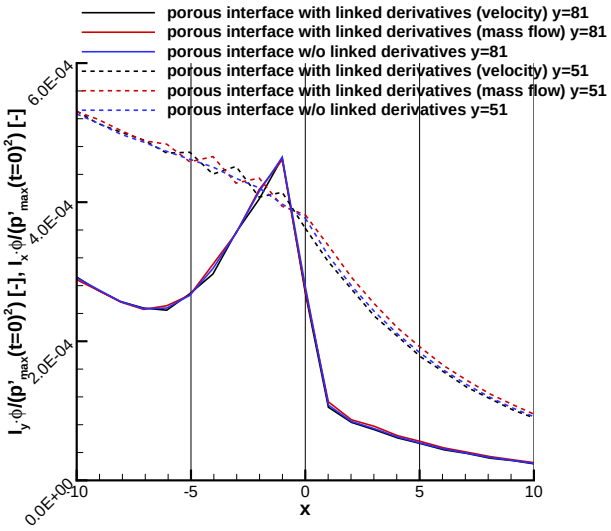

Figure 12. Acoustic intensity across the domain interface with different realizations of jump conditions along two lines at $y = 51$ (dashed lines, x-component of intensity) and $y = 81$ (solid lines, y-component of intensity).

Fig. 11 shows the result for the interface formulation with continuity of the primitive variables. Both graphs, giving the x-component in the center and the y-component in the top cut show a very similar behavior as before in the case with the plane wave. Note, that now the intensity drops according to the inverse of the distance to the initial location due to the two dimensional character. Again, the jump of the intensity directly at the interface is visible with the same magnitude. For the top cut at $y = 81$ it is interesting to notice the increase of the intensity directly left of the interface. This is due to the pressure increase related to the reflection at the interface. The y-velocity is not affected by the reflection and therefore, a rise of the intensity shows.

As an intermediate result after this section, it can be stated that different interface formulations have successfully been tested and evaluated concerning their physical background.It turned out, that for subsequent application simulations, the interface conditions at porous edges should take into account the conservation of mass flow, energy and entropy. Furthermore, it turned out that no equations creating a link of the normal derivatives of the primitive variables between both sides should be considered.

V. Application Simulation Setup

With the basic understanding of the porous interface and the choice of a set of equations, results of application simulations are presented in the following. As shown by Rossian et al.,[7] the beneficial effect of a porous trailing edge on the emitted trailing edge noise from an airfoil can be easily evaluated by the simulation of a single analytical vortex that is convected inside the boundary layer of a NACA0012 airfoil. However, these simulations were run with the porous interface conditions realizing continuous primitive variables. In the preceding sections, it was shown that this approach is too dissipative and therefore not energy-preserving. Therefore, the simulation setup sketched in Fig. 13 was reexamined with the new formulation of jump conditions. The flow parameters were set to a Mach number of $Ma_\infty = 0.15$, Reynolds number of $Re = 1.3 \cdot 10^6$ and an angle of attack of $\alpha = 0°$. The Gaussian vortex used is determined by equation Eq. (18). With this, the actual influence of the realized interface conditions on the predicted trailing edge noise reduction is evaluated anew.

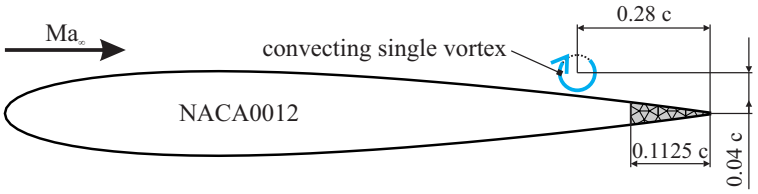

Figure 13. Simulation setup of a NACA0012 airfoil with a single analytical vortex placed inside the boundary layer ($\alpha = 0°$, $\mathbf{Ma_\infty = 0.15}$ and $\mathbf{Re = 1.3e6}$).[7]

$$\vec{v'} = 5 \cdot 10^{-3} e_\psi \times (\vec{x} - \vec{x^c}) \frac{(e \ln(4))^{\frac{1}{2}}}{8 \cdot 10^{-4}} \exp\left[- \ln 2 \frac{(\vec{x} - \vec{x^c})^2}{64 \cdot 10^{-8}} \right] \tag{18}$$

To be able to compare the numerically predicted noise reduction with experimental data, continuative simulations are run that are based on reconstruction of the turbulent eddies interacting with the airfoil's trailing edge. Here, the simulation method FRPM (Fast Random Particle Mesh Method)[10] is used in combination with solving the acoustic perturbation equations (APE).

VI. Application Results

This section presents the simulation results of the NACA0012 airfoil with solid and porous trailing edge. As described before, two setups are used to qualify the influence of the different materials. First, a simulation solving the LEE with a single analytical vortex convected along the mean flow around the airfoil is run. Then, the turbulence reconstruction method FRPM is applied to generate the turbulence related acoustic sources. The acoustic field then is given by the APE. Note, that different from the test cases before, now the mean flow is considered for the jump formulations of the porous interface.

VI.A. Single Vortex Simulations

Figs. 14 and 15 show the time signals of the acoustic fluctuating pressure registered at a microphone position 90° above the trailing edge at a distance of $1 \cdot c$ for a solid and different porous trailing edges. Here, only homogeneous, isotropic materials are investigated. For the effect of complex porous materials see Rossian et al.[7] In both figures, the plotted acoustic pressure is normalized by the linearized dynamic pressure of the set vortex. Apart from this normalization, the results shown in Fig. 14 are the same as in a previous publication.[7] They show a general beneficial influence of the porous material on the emitted trailing edge noise. For example, the material with a permeability of $\kappa = 10^{-10}\mathrm{m}^2$ gives a noise reduction of about 3.5 dB and furthermore, a significant decrease for higher permeable materials is obtained. Note, that there is a natural limit to the noise reduction potential of homogeneous materials, as for highly permeable materials a secondary sound source becomes prominent. This secondary source can be related to the beginning of the porous material. There, a new artificial trailing edge is created from the discontinuous transition from solid airfoil to permeable material. This can be seen at a simulation time of 0.0027 s.

Comparing Fig. 15 to the previous results, one notes that the achieved noise reduction diminishes for all porous materials when the jump conditions without link of the derivatives are used. This seem appropriate,

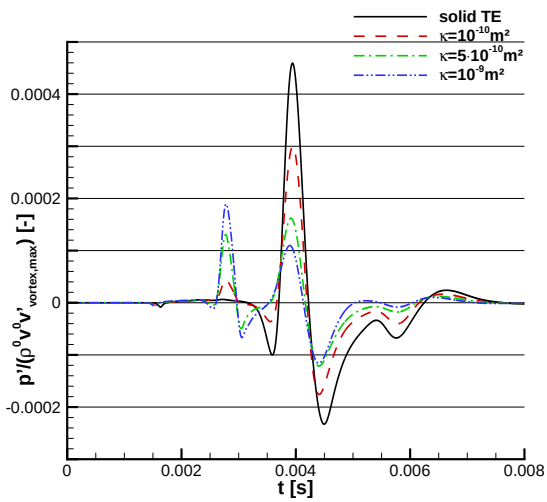

Figure 14. Time signal of the trailing edge noise emitted from a NACA0012 airfoil with solid and different porous trailing edges registered by a microphone located 90° above the trailing edge at a distance of $1 \cdot c$. Sound source realized by a single vortex and porous interface formulation with continuity of primitive variables without link of derivatives.[7]

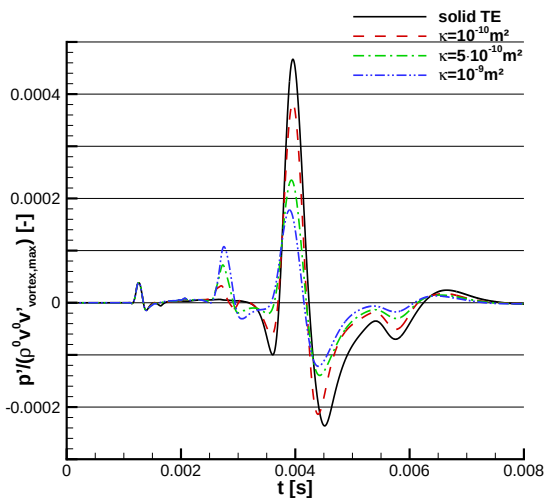

Figure 15. Time signal of the trailing edge noise emitted from a NACA0012 airfoil with solid and different porous trailing edges registered by a microphone located 90° above the trailing edge at a distance of $1 \cdot c$. Sound source realized by a single vortex and porous interface formulation with jump conditions without link of derivatives.

as in section IV.B.2 it was shown that the formulation with continuous primitive variables across the porous interface is too dissipative. Therefore, energy is lost and thus not available for the radiated acoustic waves. However, the overall characteristic effect of the porous materials is preserved. In the new simulations, one can identify an analogous reduction of the main pressure peak that lies in the order of 2 dB and increases significantly for highly permeable materials as before. Also the upcoming secondary source at the beginning of the porous material is visible but does not become dominant for the shown material parameters. As the jump interface conditions have the same effect as an artificial reduction of the permeability in comparison to the previously found results with continuous primitive variables, it is plausible to assume that here exists a similar limit to the noise reduction potential.

The above shown simulation results are altogether consistent, but have not yet been compared to experimental data. Therefore, the next section will show simulation results not with a single vortex, but acoustic sources that are based on the turbulence statistics of the CFD-simulations.

VI.B. Turbulence Reconstruction Simulations

As mentioned before, to compare the numerically predicted influence of a porous trailing edge to experimental data, simulations of a NACA0012 airfoil with reconstructed turbulence are run. The parameters of the porous region of the airfoil represent a porous aluminum (PA80), that has been investigated by Herr et al.[3] on a DLR F16 airfoil. As the run simulations were two dimensional, the resulting absolute sound pressure levels are naturally not comparable to the measured levels. Therefore, Fig. 16 gives a qualitative comparison. It is important to mention, that a constant offset between numerical and experimental data was assumed, so the noise reduction effect of the porous trailing edge is directly comparable. The numerical setup was realized with the jump formulation of the porous trailing edge without coupling of the derivatives, as the preceding investigations have shown that this formulation seems to relate best to the physical understanding of such interface.

Fig. 16 reveals, that the numerically predicted noise reduction effect of the porous material is in good accordance with the experimental data. For the solid case, the maximum deviation of the calculated spectrum from the measured spectrum is 2 dB at the frequency band of 5 kHz. This is probably due to the comparison of different airfoils, as the kink in the measured spectrum is specific for the DLR F16 airfoil. Apart from that, the maximum deviation is 1 dB. For the porous setup, a constant shift of the simulated spectrum of about+1 dB in relation to the measured data is visible for the realization with jump conditions at the porous interface. This is small compared to the overall sound reduction of 5-6 dB and might also be an effect of the

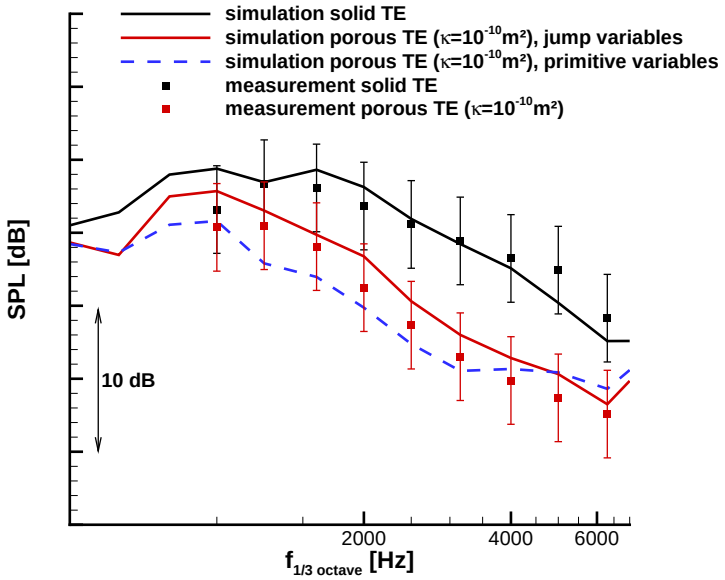

Figure 16. Third octave band spectra form FRPM simulations of a NACA0012 airfoil with solid and porous trailing edge and experimental data of a DLR F16 airfoil with the same trailing edge materials provided by Herr et al.[3]

different airfoils. The overall broadband characteristic of the achieved noise reduction by the porous trailing edge is the same for the investigated frequency range. For comparison, Fig. 16 also shows the calculated spectrum from a simulation with continuous primitive variables. As found in the previous section, lower sound pressure levels are observed. At frequencies of 1.5 kHz to 2.5 kHz the spectrum from the simulation with jump conditions shows a better match with the experimental data. For higher frequencies, the spectrum from the simulation with continuous primitive variables raises and meets the other numerically determined spectrum. This may be an effect of spurious background noise that is related to differing mesh resolutions in FRPM and PIANO. Thus this part of the spectrum should be considered carefully. Altogether, the found jump formulation for the porous interface seems to be a suitable means for trailing edge noise simulations with porous materials.

VII. Summary and Outlook

In the present paper, a reformulation of the before presented volume averaged LEE and acoustic jump conditions is presented. Then, a change in the setting of the compact boundary scheme is presented, that reduces the order of the used single-sided differentiation stencil to stabilize the system. The effect of this adjustment is then studied in a test case for the interface of identical computational sub domains. It can be shown, that the local reduction of the order has only very limited effect on the obtained propagation of the acoustic waves. For resolutions of 10 PPW and more, no drawbacks are visible.

From there on, different interface conditions to treat the edge of a porous regime are studied. As a result, a formulation taking into account the conservation variables mass flow, energy and entropy turns out to be suitable to describe the physical function of such porous interface. Note, that only a C^0-continuity is provided, as it was shown that considering the link of derivatives across the interface produces spurious noise.

With the found interface formulation simulations of the trailing edge noise of a NACA0012 airfoil are run. Thereby two simulation setups are examined. On the one hand, a single vortex convecting with the mean flow around the airfoil was used to get an insight in the sound production process. On the other hand, the turbulence reconstruction method FRPM was used to calculate sound pressure level spectra that are comparable to experimental results. Here, the results with the new interface formulation showed a different behavior than previous simulations, which can be related to the physical model behind the equations.

Furthermore, it was shown that the third octave band spectra calculated from the simulations match the experimental data for both airfoils with solid and porous trailing edge materials very well.

VIII. Acknowledgement

Financial support is provided by the German Research Foundation (Deutsche Forschungsgemeinschaft, DFG) in the framework of the Sonderforschungsbereich 880. Computational resources are provided by German Aerospace Center (Deutsches Zentrum für Luft- und Raumfahrt e.V., DLR), Institute of Aerodynamics and Flow Technology.

References

[1]Hayden, R. E. and Chanaud R.C., "Foil Structures with Reduced Sound," 1974.

[2]Herr, M., "Design Criteria for Low-Noise Trailing-Edges," AIAA Paper 2007-3470, 2007.

[3]Herr, M., Rossignol, K.-S., Delfs, J. W., Mößner, M., and Lippitz, N., "Specification of Porous Materials for Low-Noise Trailing-Edge Applications," AIAA Paper 2014-3041, 2014.

[4]Faßmann, B., Rautmann, C., Ewert, R., and Delfs, J. W., "Prediction of Porous Trailing Edge Noise Reduction via Acoustic Perturbation Equations and Volume Averaging," AIAA Paper 2015-2525, 2015.

[5]Rossian, L., Faßmann, B. W., Ewert, R., and Delfs, J. W., "Prediction of Porous Trailing Edge Noise Reduction Using Acoustic Jump-Conditions at Porous Interfaces," AIAA Paper 2016-2920, 2016.

[6]Kumar, P., Kutscher, K., Mößner, M., Radespiel, R., Krafczyk, M., and Geier, M., "Validation of a VRANS-Model for Turbulent Flow over a Porous Flat Plate by Cumulant-Lattice-Boltzmann DNS/LES and Experiments," *Journal of Porous Media*, 2017, accepted for publication.

[7]Rossian, L., Ewert, R., and Delfs, J. W., "Prediction of Porous Trailing Edge Noise Reduction by Application of Complex Porous Material," *New Results in Numerical and Experimental Fluid Mechanics XI*, edited by A. Dillmann, G. Heller, E. Krämer, R. Radespiel, and C. Wagner, Springer, 2017.

[8]Ewert, R. and Schröder, W., "Acoustic perturbation equations based on flow decomposition via source filtering," *Journal of Computational Physics*, Vol. 188, No. 2, 2003, pp. 365–398.

[9]Mößner, M. and Radespiel, R., "Modelling of turbulent flow over porous media using a volume averaging approach and a Reynolds stress model," *Computers & Fluids*, Vol. 108, 2015, pp. 25 – 42.

[10]Ewert, R., Dierke, J., Siebert, J., Neifeld, A., Appel, C., Siefert, M., and Kornow, O., "CAA broadband noise prediction for aeroacoustic design," *Journal of Sound and Vibration*, Vol. 330, No. 17, 2011, pp. 4139–4160.